ISSN 1560-3547, Regular and Chaotic Dynamics, 2013, Vol. 18, No. 3, pp. 214–225. © Pleiades Publishing, Ltd., 2013.

Generalized Synchronization of Identical Chaotic Systems on the Route from an Independent Dynamics to the Complete Synchrony

Alexey Yu. Jalnine*

Saratov Branch of Kotel'nikov's Institute of Radio-Engineering and Electronics of RAS, ul. Zelenaya 38, Saratov, 410019, Russia

Received December 12, 2012; accepted January 16, 2013

Abstract—The transition from asynchronous hyperchaos to complete synchrony in coupled identical chaotic systems may either occur directly or be mediated by a preliminary stage of generalized synchronization. In the present paper we investigate the underlying mechanisms of realization of the both scenarios. It is shown that a generalized synchronization arises when the manifold of identically synchronous states M is transversally unstable, while the local transversal contraction of phase volume first appears in the areas of phase space separated from M and being visited by the chaotic trajectories. On the other hand, a direct transition from an asynchronous hyperchaos to the complete synchronization occurs, under variation of the controlling parameter, if the transversal stability appears first on the manifold M, and only then it extends upon the neighboring phase volume. The realization of one or another scenario depends upon the choice of the coupling function. This result is valid for both unidirectionally and mutually coupled systems, that is confirmed by theoretical analysis of the discrete models and numerical simulations of the physically realistic flow systems.

MSC2010 numbers: 34D06, 34D08, 34D20, 34D30, 37C60, 37C70, 37B25, 37D05, 37D45

DOI: 10.1134/S1560354713030027

Keywords: synchronization, chaotic dynamics, strange attractors

1. INTRODUCTION

Synchronization of the dynamics of coupled chaotic systems is a fundamental natural phenomenon, which has been observed in many physical, chemical and biological systems. Classifying a variety of different synchronization types, the researchers usually distinguish a complete synchronization of identical systems [1–5] and a generalized synchronization of non-identical ones [2, 6–8]. For more detailed classification of the synchronization phenomena including phase and lag synchronization etc., see survey works [9, 10].

In the case of a vanishing coupling between individual chaotic systems, their asynchronous dynamics corresponds to existence of a hyperchaotic (i.e. characterized by two or more of positive Lyapunov exponents) attractor in the joint phase space. An appearance of a complete or generalized synchronization suggests that the chaotic motion becomes restricted to an invariant subspace of the whole phase space. In the case of a complete synchronization of a pair of identical chaotic systems, a synchronous chaotic attractor exists on the trivial manifold of identical states $M : \{(\mathbf{x}, \mathbf{y})|\mathbf{x} = \mathbf{y}\}$, where $\mathbf{x}$ and $\mathbf{y}$ are the state vectors of individual systems. If this attractor is stable against perturbations transverse to the manifold M (i.e. all the transversal Lyapunov exponents characterizing the attractor are negative), it may become an attractor in the whole phase space. For the case of a generalized synchronization, the identity of the individual systems dynamics is not required, instead a relationship of a general form between systems states is necessary [2, 10]. In the majority of studies of generalized synchronization phenomena, the model is represented by the example of a pair of unidirectionally coupled systems [6–8]. As the criteria of existence of a

*E-mail: Jalnine@rambler.ru

generally synchronous regime, the method of negative conditional Lyapunov exponents [7] and the auxiliary system method [11] are usually used. The main point of the both methods consists in that (for definiteness suggest that the system "$\mathbf{x}$" is a driving and "$\mathbf{y}$" is a response one), independently of an initial state $\mathbf{y}(t_0)$ of the response system, it approaches the state uniquely defined by the driving system after sufficiently long time term: $\mathbf{y}(t) \to \mathbf{f}(\mathbf{x}(t))$ at $t \to \infty$.

However, it is known, that identical chaotic systems may also demonstrate such a type of dynamics, when the systems states are not identical, but there is a functional relationship between them, and the corresponding Lyapunov exponents take on negative values. In particular, such situation was observed for unidirectionally coupled identical systems in Refs. [12–14]. Obviously, this satisfies the definition of synchronization in a generalized sense. Such a situation may arise on the route of transition from an asynchronous hyperchaos to a completely synchronous chaos, as it was shown in Ref. [15], and as it follows from the details of transitions described in Refs. [16–19]. Thus, the generalized synchronization stands as an intermediate type of dynamics on the route from independent behavior to a complete synchrony. On the other hand, this scenario is not universal [20], and a direct transition from asynchronous hyperchaos to completely synchronous chaos without intermediate stage of generalized synchronization is also possible for both unidirectionally [21–23] and symmetrically [24–26] coupled systems. The question about special conditions which result in the choice of one or another of the scenarios described above is still unrevealed and represents an actual interest.

The purpose of the present paper is an investigation of the general mechanism responsible for realization of the both direct and indirect scenarios of the transition from independent hyperchaotic dynamics to the complete chaos synchronization. For rigorous theoretical analysis, we construct a transparent model of generalized synchronization in the form of a pair of coupled identical discrete maps of special type, demonstrating chaos in individual dynamics, with a controllable type and direction of coupling, which can be chosen both unidirectional and mutual. By example of this model, we show analytically that two conditions are necessary for appearance of the generalized synchronization: (i) the transversal instability of chaotic trajectories on the manifold M and (ii) the existence of areas of the local transversal contraction of phase volume isolated from M and being visited by trajectories of the chaotic attractor. The specific choice of scenario of the transition from asynchronous hyperchaos to identically synchronous chaos then depends upon the order of appearance of transversal stability on the manifold M and in the adjoining regions of the phase space, under variation of the controlling parameter of the transition. If the transversal stability appears on the manifold M first as the controlling parameter is varied, and then it extends to the manifold's neighborhood, the direct transition from asynchronous hyperchaos to completely synchronous chaos is observed. On the other hand, if the local transversal stability appears first in the regions being visited by chaotic trajectories and isolated from M, and only then the manifold becomes transversally stable, the generalized synchronization arises as an intermediate type of dynamics on the route of such transition. The realization of one or another scenario in our model depends upon the choice of coupling function, which can provide an appearance of local transversal contraction of phase volume in a vicinity of the manifold M or in some other regions of the phase space. The analysis of the models with different directions of coupling shows that our results are valid for both unidirectionally and mutually (asymmetrically or symmetrically) coupled systems.

In order to demonstrate the universality of conclusions obtained from theoretic analysis, we also consider a physically realistic flow model consisting of a pair of coupled chaotic oscillatory systems, which individually possess robust chaotic dynamics [27] with a hyperbolic attractor of the Smale–Williams type. Introducing different types and directions of coupling in this flow, we numerically observe exactly the same picture of the transition scenarios, that was previously observed theoretically for the models in the form of coupled maps.

2. THE DISCRETE MODELS

The basic subsystem which will be used for theoretical analysis is the most simple chaotic map, known as the Bernoulli map: $x' = 2x \pmod{2\pi}$. Let us consider a pair of coupled maps of this type:

$$\begin{aligned} x' &= 2x + (\alpha - 1)Cg(x - y) \pmod{2\pi}, \\ y' &= 2y + Cg(x - y) \pmod{2\pi}, \end{aligned} \tag{2.1}$$

where C is a parameter of coupling strength, and $g(v)$ is a coupling function which satisfies the following conditions: (i) $g(0) = 0$ (zero effect on the invariant diagonal $M : \{(x, y)|x = y\}$, (ii) $g(v) = -g(-v)$ (asymmetry by the variable), (iii) $g(v) = g(v + 2\pi)$ and $D^n g(v) = D^n(v + 2\pi)$ at $n \in N$ (continuity and differentiability at the points of joining). In the simplest case such function can be chosen in the sinusoidal form:

$$g(v) = \sin v. \tag{2.2}$$

For $\alpha = 0$ the coupling becomes symmetric, while for nonzero α ($0 < \alpha \leqslant 1$) it is asymmetric. The extreme case of asymmetric coupling with $\alpha = 1$ corresponds to the unidirectional coupling. In such a way, α tunes the degree of asymmetry in the coupling.

For convenience, let us proceed to the longitudinal and transversal variables ($u = x + y$, $v = x - y$) and then rewrite the system (2.1) as

$$\begin{aligned} u' &= 2u + \alpha C g(v) \pmod{2\pi}, \\ v' &= 2v + (\alpha - 2) C g(v) \pmod{2\pi}. \end{aligned} \tag{2.3}$$

From Eqs. (2.3) it immediately follows that the original system (2.1), (2.2) is characterized by two Lyapunov exponents $\lambda_{||} = \ln 2$ and $\lambda_\perp =< \ln |2 - C^* \cos v| >$ (here and thereafter we denote $C^* = (2 - \alpha)C$), which measure the longitudinal and transversal (in)stability of any trajectory. Then, for trajectories on the diagonal the value of the transversal exponent is $\lambda_\perp = \ln |2 - C^*|$. Hence, the transition to the complete synchronization under increasing of the coupling parameter occurs at $C^* = C^*_f = 1.0$. The examples of phase portraits of the map (2.1), (2.2) for the case of the symmetric coupling just prior and immediately beyond the transition are shown in Figs. 1a and 1b, respectively. From Fig. 1a one can see the crowding of the phase trajectories in vicinity of the diagonal, which then becomes transversally stable. The plots of the dependences of Lyapunov exponents vs. C^* are shown in Fig. 1c. The plot $\lambda_\perp(C^*)$ for attractor is shown in black, while the plot $\lambda_\perp(C^*)$ for repeller on the diagonal is shown in grey. From the latter figure one can immediately see, that the transition to the complete synchronization occurs directly, without intermediate stage of generalized synchronization, which would be characterized by negative value of $\lambda_\perp$ for attractor simultaneously with the positive $\lambda_\perp$ for the repeller. In order to understand the reason of such behavior, let us consider the value of a finite-time ("local") transversal exponent taken per one iteration: $\Lambda_\perp(v) = \ln |2 - C^* \cos v|$. For any C^* within the interval $C^* \in [0, 2)$, the minimum value of the function $\Lambda_\perp(v)$ falls on $v = 0$ (see a typical plot in Fig. 1d for $C^* = C^*_f$). Hence, as the parameter C^* passes the critical value C^*_f, the transversal stability first arises on the diagonal, and only then it extends upon other regions of the whole phase space. Obviously, the reason for direct transition to the complete synchrony in our situation consists in the choice of the coupling function in the sinusoidal form, which minimizes the local transversal exponent on the invariant diagonal M. Therefore, in order to observe the indirect transition to the complete synchrony through an intermediate stage of the generalized synchronization, one should select the coupling function in such a way that the local transversal exponent would take minimum value in some other region of the phase space, instead of the diagonal M.

Let us modify the coupling function in a following way:

$$g(v) = [1 + B \sin^2 v] \sin v. \tag{2.4}$$

The idea of this modification consists in the modulation of the sinusoidal function by the factor, which has the minimum value at $v = 0$, and which increases sufficiently as v is varied from zero. In this case the effect of transversal contraction will be stronger in the regions distant from the diagonal. Then, for local transversal Lyapunov exponent we obtain:

$$\Lambda_\perp(v) = \ln |2 - C^*(\cos v + 3B \sin^2 v \cos v)|. \tag{2.5}$$

One can easily see that the value of this exponent on the diagonal remains the same: $\Lambda_\perp(0) = \ln |2 - C^*|$. An elementary analysis shows, that for $B > 1/6$ the function $\Lambda_\perp(v)$ has two minimums at $v_{min} = \pm \arctan \sqrt{(6B - 1)/(3B + 1)}$ and a local maximum at $v = 0$. Hence, if the parameter $C^* < C^*_f$ is chosen appropriately, the situation may arise, when $\Lambda_\perp(0) > 0$, while $\Lambda_\perp(v) < 0$ for

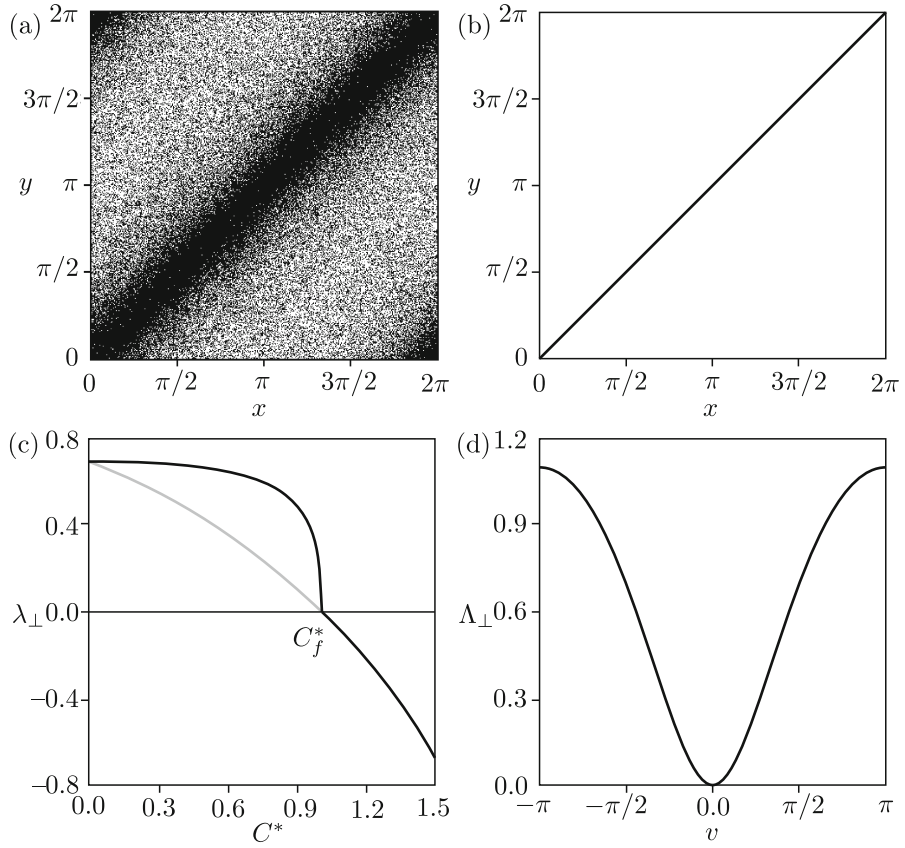

Fig. 1. The phase portraits of the system (2.1), (2.2) with symmetric coupling ($\alpha = 0$) at (a) $C = 0.49$ and (b) $C = 0.51$. (c) The dependences of transversal Lyapunov exponent $\lambda_\perp$ vs. parameter C^* for the attractor (black) and for the repeller on the diagonal (grey). (d) The dependence of local transversal exponent $\Lambda_\perp$ vs. the variable v at $C^* = 1.0$.

$v \in (v_{min} - \varepsilon, v_{min} + \varepsilon)$, that suggests appearance of local transversal stability of motion at these values of deviation from the diagonal. The corresponding example of the plot of the function $\Lambda_\perp(v)$ for $B = 1.5, C^* = 0.6$ is presented in Fig. 2a. Since the transversal instability of motion on the diagonal there takes place simultaneously with the local transversal stability arising in some neighboring regions of the phase space, one can expect, that the generalized synchronization may there appear.

The plot of the dependence of $\lambda_\perp$ vs. C^* for $B = 1.5$ is shown in Fig. 2b. From this plot one can see, that for $C^* \in (C_g^*, C_f^*)$ the condition $\lambda_\perp < 0$ for the attractor holds, although the diagonal is still transversally unstable. Hence, the dynamical regime existing in the system (2.1), (2.4) at these values of C^* is different from identical synchronization, although it is characterized by a negative transversal Lyapunov exponent. The phase portraits of the system (2.1), (2.4) with symmetric coupling ($\alpha = 0$) for hyperchaotic regime at $B = 1.5, C = 0.27$ and for the generally synchronous chaotic regime at $B = 1.5, C = 0.29$ are presented in Figs. 2c and 2d, respectively. One can observe how the chaotic trajectories condense in the regions aside from the diagonal at the threshold of the transition. After the generalized synchronization has arisen, the chaotic attractor fills the straight line segment which is parallel to the diagonal and is different from it, so that the condition holds: $x - y = \text{const}[\neq 0]$. The existence of such a trivial one-to-one functional dependence of systems variables is a sufficient criterion for detection of generalized synchronization. In order to understand the underlying cause for this trivial relationship, let us consider the dynamics of the transversal variable v described by the second equation of the system (2.3). From this equation (taken jointly with condition (2.4)) we immediately obtain, that the value of $v = \text{const}$ can be found as a solution of the transcendent equation:

$$v = C^* \sin v(1 + B \sin^2 v). \tag{2.6}$$

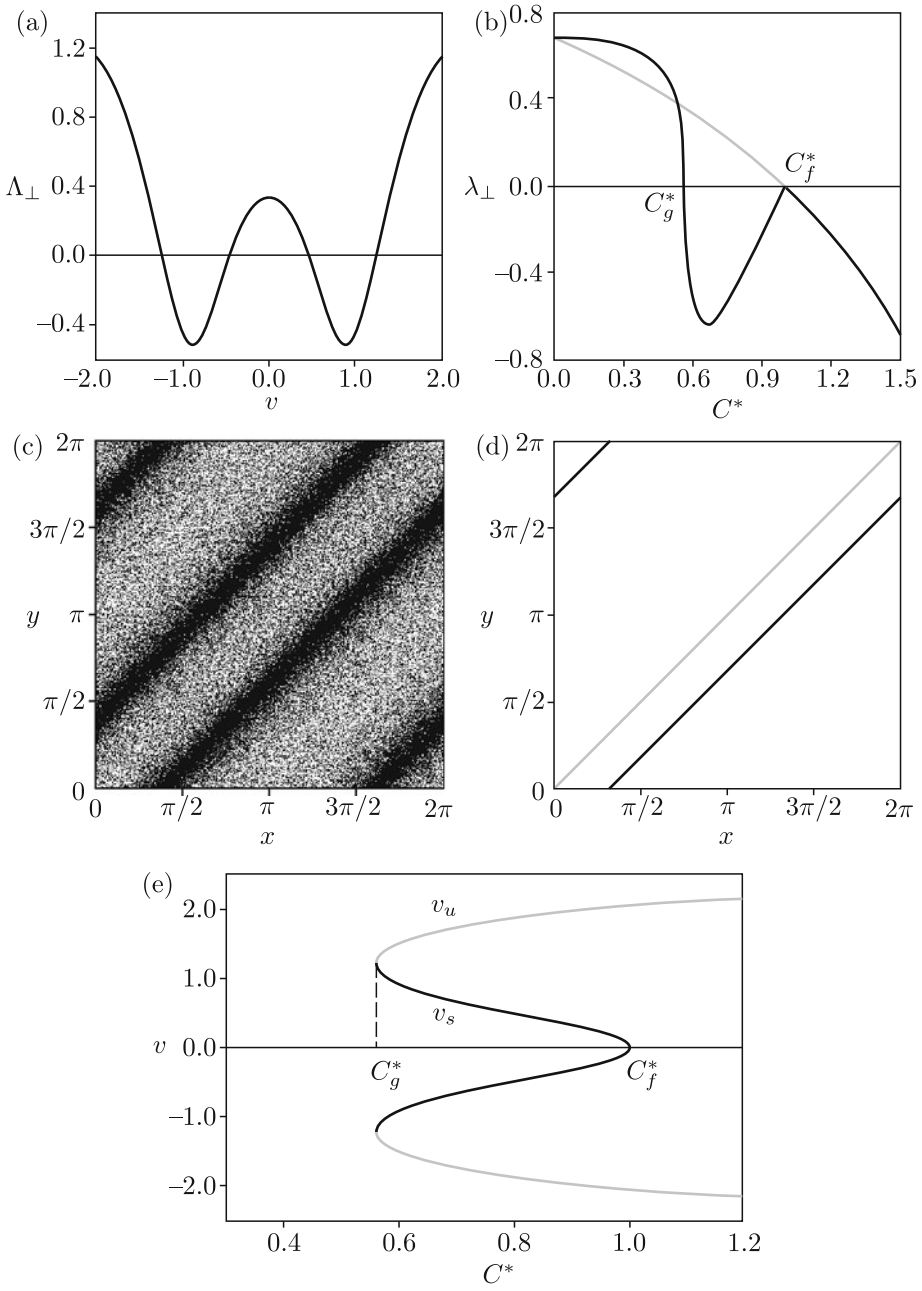

Fig. 2. (a) The dependence of local transversal exponent $\Lambda_\perp$ given by formula (2.5) vs. the variable v at $B = 1.5$ and $C^* = 0.6$. (b) The dependences of transversal Lyapunov exponent $\lambda_\perp$ vs. the parameter C^* at $B = 1.5$ for the attractor (black) and for the repeller on the diagonal (grey). The phase portraits of the system (2.1), (2.4) with symmetric coupling ($\alpha = 0$) and $B = 1.5$ at (c) $C = 0.27$ and (d) $C = 0.29$. (e) The bifurcational tree of the solutions of Eq. (2.6) for $B = 1.5$.

Thus, the investigation of the dynamics of synchronous chaotic regime of the system (2.1), (2.4) has reduced to the investigation of the solutions of Eq. (2.6). The corresponding bifurcational tree for $B = 1.5$ is presented in Fig. 2e. The branches of stable and unstable solutions are shown in black and grey, respectively. For $C^* \in [0, C_g^*)$ Eq. (2.6) has only one unstable solution: $v = 0$. At $C^* = C_g^* \approx 0.55904$ a symmetric pair of saddle-node bifurcations occurs, which results in appearance of two other pairs of the solutions, namely, two stable ($\pm v_s$) and two unstable ($\pm v_u$) ones. For $C^* \in (C_g^*, C_f^*)$ the stable solutions determine the manifolds of generally synchronous states for the map (2.1), (2.4): $x - y = \pm v_s$. At $C^* = C_f^* = 1.0$ the backward pitchfork bifurcation occurs, so that

the stable pair of solutions $\pm v_s$ disappears, while the trivial solution $v = 0$ becomes stable. This is the moment, when the regime of the complete chaos synchronization in the system (2.1), (2.4) arises.

Note, that all the above arguments illustrated by the example of symmetric coupling ($\alpha = 0$) in fact do not depend upon the choice of the parameter α, so that our results are valid for both asymmetric and unidirectional cases of mutually coupled systems as well. Therefore, the condition of appearance of generalized synchronization that we have found gives a goal-directed algorithm for construction of the regimes of generalized synchronization in identical chaotic systems with different types of mutual coupling on the route from asynchronous hyperchaos to the complete synchronization. This result is also worthy of notice, since in a usual situation, the diagnostics of the existence of generalized synchronization for bidirectionally coupled systems is rather difficult, so that the construction of the regimes with the predetermined properties may be useful for development of common methods of diagnostics of generalized synchronization in various coupled systems.

3. THE FLOW MODELS

In order to demonstrate the generality and physical meaning of the results obtained from the analysis of theoretical discrete models, let us apply the same arguments to examples of realistic flow systems. We expect to observe numerically nearly the same picture of dynamical transitions, that was described in the previous section. As a basis for modeling, we will use a non-autonomous oscillatory system, consisting of two interacting van der Pol oscillators with the characteristic frequencies of generation deferring twice, with the excitation parameters undergoing slow periodic counter-phase modulation in time, and with a special type of connection between the oscillators, which provides the forwarding of the oscillation's phase. This system was first suggested in the Ref. [27] as an example of a feasible flow with a robust chaotic attractor, and later it was realized as an electronic device in the work [28]. The equations of the system $\dot{\mathbf{x}} = \mathbf{F}(\mathbf{x}, t)$ for vector components $\mathbf{x} = (x_1, x_2, x_3, x_4)$ have the form:

$$\begin{aligned}
\dot{x_1} &= f_1(\mathbf{x}, t) = x_2, \\
\dot{x_2} &= f_2(\mathbf{x}, t) = (A\cos(\omega_0 t/N) - x_1^2)x_2 - \omega_0^2 x_1 + \varepsilon x_3 \cos\omega_0 t, \\
\dot{x_3} &= f_3(\mathbf{x}, t) = x_4, \\
\dot{x_4} &= f_4(\mathbf{x}, t) = -(A\cos(\omega_0 t/N) + x_3^2)x_4 - (2\omega_0)^2 x_3 + \varepsilon x_1^2.
\end{aligned} \tag{3.1}$$

Here ω_0 and $2\omega_0$ are the characteristic frequencies of the first and the second oscillators, respectively, A is an amplitude of the modulated excitation parameter, N is an integer number determining the period of modulation $T = 2\pi N/\omega_0$, and ε is the parameter of the connection intensity. In this Section we set the same parameters values as in the Ref. [27] for the robust hyperbolic attractor: $A = 3.0, \varepsilon = 0.5, \omega_0 = 2\pi, N = 10$. Then, the evolution of the chaotic phase $\varphi : x_1 \sim \cos(\omega_0 t + \varphi)$, determined at discrete time moments $t_n = t_0 + nT$ (where n is integer), will approximately follow the Bernoulli map ($\varphi_{n+1} \approx 2\varphi_n \pmod{2\pi}$), as in the well-known Smale–Williams model.

Now let us consider a pair of interacting systems of the described type:

$$\begin{aligned}
\dot{\mathbf{x}} &= \mathbf{F}(\mathbf{x}, t) + C(\alpha - 1)\mathbf{g}(\mathbf{x}, \mathbf{y}), \\
\dot{\mathbf{y}} &= \mathbf{F}(\mathbf{y}, t) + C\mathbf{g}(\mathbf{x}, \mathbf{y}),
\end{aligned} \tag{3.2}$$

where $\mathbf{g}(\mathbf{x}, \mathbf{y})$ is a coupling function satisfying the conditions $\mathbf{g}(\mathbf{x}, \mathbf{x}) = 0$ and $\mathbf{g}(\mathbf{x}, \mathbf{y}) = -\mathbf{g}(\mathbf{y}, \mathbf{x})$, C and α are the parameters controlling the intensity and the direction of coupling, as in the previous Section. In the cases of $\alpha = 1$ or $\alpha = 0$ the coupling becomes unidirectional or symmetrical, respectively.

The system (3.2) is characterized by 8 nontrivial Lyapunov exponents. In order to calculate the full Lyapunov spectrum, we will first linearize the system (3.2):

$$\begin{aligned}
\dot{\tilde{\mathbf{x}}} &= \frac{\partial \mathbf{F}(\mathbf{x}, t)}{\partial \mathbf{x}}\tilde{\mathbf{x}} + C(\alpha - 1)\left[\frac{\partial \mathbf{g}(\mathbf{x}, \mathbf{y})}{\partial \mathbf{x}}\tilde{\mathbf{x}} + \frac{\partial \mathbf{g}(\mathbf{x}, \mathbf{y})}{\partial \mathbf{y}}\tilde{\mathbf{y}}\right], \\
\dot{\tilde{\mathbf{y}}} &= \frac{\partial \mathbf{F}(\mathbf{y}, t)}{\partial \mathbf{y}}\tilde{\mathbf{y}} + C\left[\frac{\partial \mathbf{g}(\mathbf{x}, \mathbf{y})}{\partial \mathbf{x}}\tilde{\mathbf{x}} + \frac{\partial \mathbf{g}(\mathbf{x}, \mathbf{y})}{\partial \mathbf{y}}\tilde{\mathbf{y}}\right].
\end{aligned} \tag{3.3}$$

For the case of unidirectional ($\alpha = 1$) coupling the full set of exponents may be divided into two subsets: $\left\{\lambda_x^{(i)}\right\}_{i=1,\ldots,4}$ for characterization of the driving system "$\mathbf{x}$", and $\left\{\lambda_y^{(i)}\right\}_{i=1,\ldots,4}$ for characterization of the response system "$\mathbf{y}$". For the case of mutual ($0 \leqslant \alpha < 1$) coupling, it is impossible to distinguish the subsets associated with one or another system, and it is necessary to consider the set $\left\{\lambda^{(i)}\right\}_{i=1,\ldots,8}$ as a whole. The procedure for calculation of the values of $\left\{\lambda_x^{(i)}\right\}_{i=1,\ldots,4}$ based on Benettin's algorithm is fully described in Ref. [27]. For this purpose one should assign an orthonormal basis of 4 vectors $\left\{(\tilde{x}_1^{(i)}(t), \tilde{x}_2^{(i)}(t)/\omega_0, \tilde{x}_3^{(i)}(t), \tilde{x}_4^{(i)}(t)/2\omega_0)\right\}_{i=1,\ldots,4}$ at the time moment $t = t_0$, and then consider the evolution of these vectors under the effect of the first equation of the system (3.3) being integrated jointly with the corresponding equation of the system (3.2). In the course of the integration, the Gram–Schmidt orthogonalization and normalization must be performed at time moments $t_n = t_0 + nT$. Summing up the logarithms of the norms (after the orthogonalization, but before the normalization), one can obtain the values of exponents $\left\{\lambda_x^{(i)}\right\}_{i=1,\ldots,4}$ as the mean rates of growth or decrease of the accumulated sums. In accordance with the results of the Ref. [27], the value of the largest exponents in this set is $\lambda_x^{(1)} \approx T^{-1} \ln 2 \approx 0.068$, while other ones are sufficiently negative and depend upon the choice of the parameters of the basis subsystem (3.1). For calculation of the values of $\left\{\lambda_y^{(i)}\right\}_{i=1,\ldots,4}$ one should assign the orthonormal basis of 4 vectors $\left\{(\tilde{y}_1^{(i)}(t), \tilde{y}_2^{(i)}(t)/\omega_0, \tilde{y}_3^{(i)}(t), \tilde{y}_4^{(i)}(t)/2\omega_0)\right\}_{i=1,\ldots,4}$ at the time moment $t = t_0$. Note, that all the values of variations "$\tilde{x}$" in the second equation of the system (3.3) must be set to zero (i.e. $\left\{\tilde{x}_1^{(i)}(t) = 0, \tilde{x}_2^{(i)}(t) = 0, \tilde{x}_3^{(i)}(t) = 0, \tilde{x}_4^{(i)}(t) = 0\right\}_{i=1,\ldots,4}$). Then, this equation must be integrated jointly with the system (3.2). Performing orthogonalization and normalization via Gram–Schmidt scheme at time moment $t_n = t_0 + nT$, we will obtain the values of exponents $\left\{\lambda_y^{(i)}\right\}_{i=1,\ldots,4}$ of the response system as the mean values of the logarithms of the vector norms taken after the orthogonalization and before the normalization.

In the same way one can find the whole set of $\left\{\lambda^{(i)}\right\}_{i=1,\ldots,8}$ for the case of mutual coupling of the systems. For this purpose one should assign a basis consisting of 8 vectors $\left\{(\tilde{x}_1^{(i)}(t), \tilde{x}_2^{(i)}(t)/\omega_0, \tilde{x}_3^{(i)}(t), \tilde{x}_4^{(i)}(t)/2\omega_0, \tilde{y}_1^{(i)}(t), \tilde{y}_2^{(i)}(t)/\omega_0, \tilde{y}_3^{(i)}(t), \tilde{y}_4^{(i)}(t)/2\omega_0)\right\}_{i=1,\ldots,8}$ at the time moment $t = t_0$, and then consider the evolution of these vectors under the effect of the whole system of Eqs. (3.3) being integrated jointly with the whole system (3.2). As previously, performing the Gram–Schmidt orthonormalization and averaging the logarithms of norms of the vectors (after the orthogonalization but before the normalization), one can obtain the values of $\left\{\lambda^{(i)}\right\}_{i=1,\ldots,8}$.

Using the procedures described above, let us characterize the scenarios of transition from asynchronous hyperchaos to completely synchronous chaos for the system (3.2) with various types of coupling in terms of Lyapunov exponents. Constructing the coupling function, we will proceed from the same arguments, which were used for the case of the discrete models (see formula (2.4)), with the only difference consisting in that we do not need a 2π-periodicity of the function by the variables. Let us define the coupling function $\mathbf{g}(\mathbf{x}, \mathbf{y})$ in the following form:

$$g_i(\mathbf{x}, \mathbf{y}) = (x_i - y_i)[1 + B(x_i - y_i)^2], \quad i = 1, \ldots, 8. \tag{3.4}$$

For the case of $B = 0$ the coupling becomes linear. For $B > 0$ the linear term is modulated by the factor, which has minimum on the manifold of synchronous states $M : \{(\mathbf{x}, \mathbf{y}) | \mathbf{x} = \mathbf{y}\}$, and which growths with the transversal deviation of the trajectory from M. Note also, that the coupling function in the chosen form satisfies the condition: $\partial \mathbf{g}(\mathbf{x}, \mathbf{y})/\partial \mathbf{x} = -\partial \mathbf{g}(\mathbf{x}, \mathbf{y})/\partial \mathbf{y}$.

In order to determine the threshold of the complete synchronization appearance, let us consider the dynamics of the system (3.2) with condition (3.4) on the manifold of synchronous states M. It is possible to obtain analytically the functional dependences of the Lyapunov exponents upon the parameters of coupling for an attractor/saddle on the manifold M, if we proceed to the longitudinal

and transversal variables ($\mathbf{u} = \mathbf{x} + \mathbf{y}$,$\mathbf{v} = \mathbf{x} - \mathbf{y}$) in the system (3.2) and correspondingly rewrite the linearized system (3.3). Then, for a synchronous chaotic trajectory $\mathbf{x}^*(t) = \mathbf{y}^*(t)$ taken as the reference one, we will obtain the linearized system for new variables:

$$\begin{aligned} \dot{\tilde{\mathbf{u}}} &= \left[\frac{\partial \mathbf{F}(\mathbf{x},t)}{\partial \mathbf{x}}\right]_{\mathbf{x}=\mathbf{x}^*} \tilde{\mathbf{u}} + \alpha C \hat{\mathbf{h}}(\mathbf{x}^*,\mathbf{y}^*)\tilde{\mathbf{v}}, \\ \dot{\tilde{\mathbf{v}}} &= \left[\frac{\partial \mathbf{F}(\mathbf{x},t)}{\partial \mathbf{x}}\right]_{\mathbf{x}=\mathbf{x}^*} \tilde{\mathbf{v}} + (\alpha-2) C \hat{\mathbf{h}}(\mathbf{x}^*,\mathbf{y}^*)\tilde{\mathbf{v}}. \end{aligned} \tag{3.5}$$

Here $\hat{\mathbf{h}}(\mathbf{x},\mathbf{y}) = \partial \mathbf{g}(\mathbf{x},\mathbf{y})/\partial \mathbf{x}$ is a linear matrix operator with the components $h_{i,j}(\mathbf{x},\mathbf{y})$, $i,j = 1,\ldots,4$. From the definition of the coupling function via formula (3.4) it immediately follows that $\hat{\mathbf{h}}(\mathbf{x}^*,\mathbf{y}^*) = \delta_{ij}$.

The system (3.5) formally represents a pair of subsystems with unidirectional coupling. Therefore, the whole set of 8 Lyapunov exponents can be divided there into two subsets of longitudinal exponents $\left\{\lambda_{||}^{(i)}\right\}_{i=1,\ldots,4}$ associated with the variable $\mathbf{u}$, and transversal exponents $\left\{\lambda_{\perp}^{(i)}\right\}_{i=1,\ldots,4}$ associated with the variable $\mathbf{v}$, for which the conditions hold:

$$\lambda_{||}^{(i)} = \lambda_x^{(i)}, \quad \lambda_{\perp}^{(i)} = \lambda_x^{(i)} + (\alpha-2)C, \quad i = 1,\ldots,4, \tag{3.6}$$

where $\left\{\lambda_x^{(i)}\right\}_{i=1,\ldots,4}$ coincide with the exponents characterizing the original single subsystem (3.1). Correspondingly, for the case of the unidirectional coupling ($\alpha = 1$) the complete synchronization arises at $C_f = \lambda_x^{(1)} \approx T^{-1}\ln 2$, while for the case of the symmetric coupling ($\alpha = 0$) it appears at $C_f = \lambda_x^{(1)}/2 \approx (2T)^{-1}\ln 2$.

At first, let us illustrate the direct transition from asynchronous hyperchaos to the complete synchronization. For that, we assign $B = 0$ in formula (3.4). The plots of the dependences of selected Lyapunov exponents upon the coupling parameter C for the case of unidirectional coupling are presented in Fig. 3a. The plots of the exponents $\lambda_x^{(1)}$ and $\lambda_y^{(1)}$ for the attractor are shown in black, while the plot of $\lambda_{\perp}^{(1)}$ for the chaotic saddle on the manifold M is shown in grey. The values of other exponents are sufficiently negative and do not change noticeably on the route of the transition. Therefore, they are not presented. The synchronization arises when the largest exponent of the response system $\lambda_y^{(1)}$ passes zero value and becomes negative. From the diagram one can see that it occurs exactly at the moment when $\lambda_{\perp}^{(1)}$ passes through "0" and the manifold M becomes transversally stable. Hence, here the complete synchronization arises directly. Introducing the discrete phases for the both systems "$\mathbf{x}$" and "$\mathbf{y}$" as $\varphi_n = \arg\left[x_2(t_n) + i\omega_0 x_1(t_n)\right]$ and $\psi_n = \arg\left[y_2(t_n) + i\omega_0 y_1(t_n)\right]$, we can observe the portraits of the mappings (φ_n, ψ_n) for hyperchaotic and completely synchronous chaotic regimes as shown in Figs. 3b and 3c, respectively. From Fig. 3b one can see the crowding of the phase trajectories near the diagonal on the threshold of the transition.

In Fig. 3d the plots of the dependences of Lyapunov exponents upon the parameter C are presented for the case of the symmetric coupling (as before, we set $B = 0$). The plots for two largest exponents of the attractor $\lambda^{(1)}$ and $\lambda^{(2)}$ are shown in black, the plot for the transversal exponent $\lambda_{\perp}^{(1)}$ of the chaotic saddle on the manifold M is shown in grey. For the case of asynchronous hyperchaotic regime, the both exponents of the attractor ($\lambda^{(1)}$ and $\lambda^{(2)}$) are positive. The value of $\lambda^{(2)}$ becomes negative simultaneously with the value of $\lambda_{\perp}^{(1)}$, whereupon the complete chaos synchronization arises. The examples of phase portraits for the mapping (φ_n, ψ_n) of hyperchaotic and synchronously chaotic regimes are shown in Figs. 3e and 3f.

Next, let us consider the case of an indirect transition to the complete synchronization through the intermediate stage of the generalized synchrony. For this purpose we assign $B > 0$ in formula (3.4). Note, that relationships (3.6) for the longitudinal and transversal exponents of

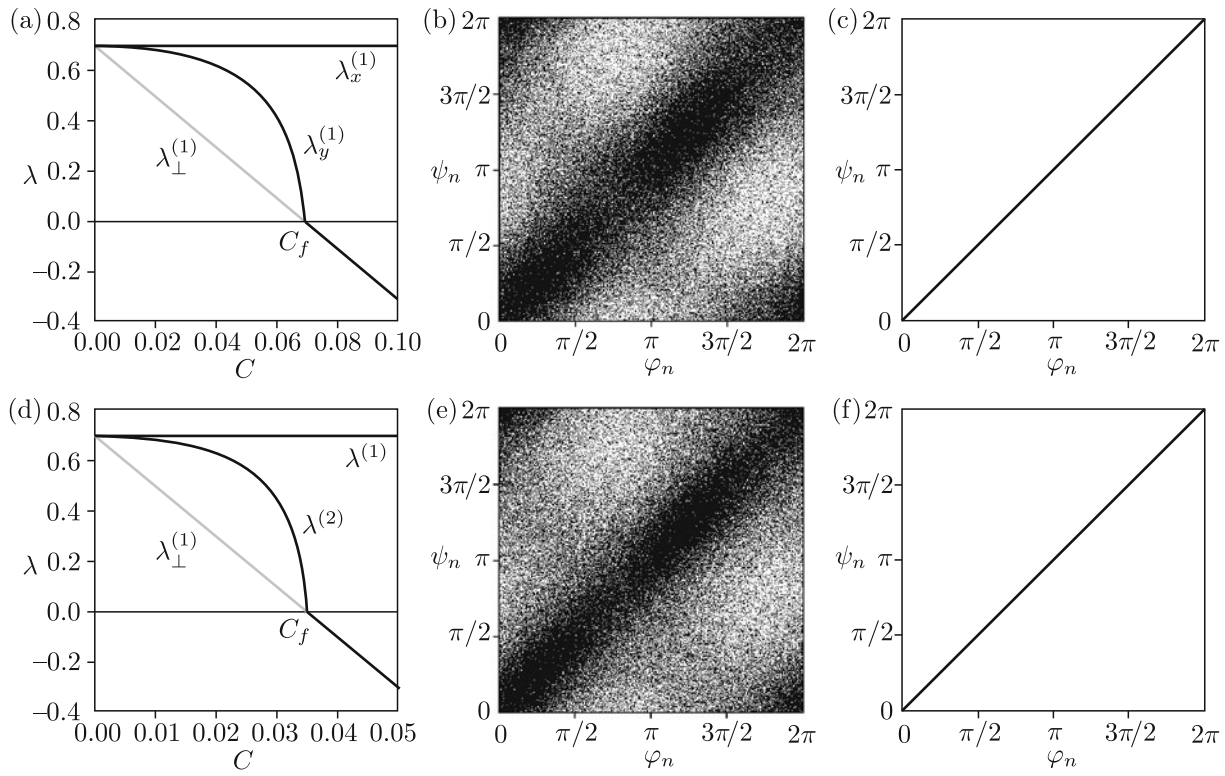

Fig. 3. (a) The dependences of Lyapunov exponents of the system (3.2), (3.4) with unidirectional linear coupling ($\alpha = 1, B = 0.0$) vs. parameter C, and the phase portraits of the mapping (φ_n, ψ_n): (b) for hyperchaotic regime at $C = 0.06$, and (c) for completely synchronously chaotic regime at $C = 0.08$. (d) The dependences of Lyapunov exponents of the system (3.2), (3.4) with symmetric linear coupling ($\alpha = 0, B = 0.0$) vs. parameter C, and the phase portraits of the mapping (φ_n, ψ_n): (e) for hyperchaotic regime at $C = 0.03$, and (f) for completely synchronous chaotic regime at $C = 0.04$.

synchronous trajectories on the manifold M then remain unchanged, as well as the thresholds of the complete synchronization $C_f = \lambda_x^{(1)} \approx T^{-1} \ln 2$ for the unidirectional coupling and $C_f = \lambda_x^{(1)}/2 \approx (2T)^{-1} \ln 2$ for the symmetric coupling.

The corresponding plots of the dependences of Lyapunov exponents upon the parameter C for the case of unidirectional coupling are shown in Fig. 4a. As previously, the plots of $\lambda_x^{(1)}$ and $\lambda_y^{(2)}$ for the attractor are shown in black, while the plot of $\lambda_\perp^{(1)}$ for the chaotic saddle on the manifold M is shown in grey. From these plots one can see that, as C is increased, the largest exponent $\lambda_y^{(2)}$ of the response system becomes negative at $C = C_g \approx 0.0414$, while the value of the transversal exponent of the chaotic saddle $\lambda_\perp^{(1)}$ remains positive. Hence, according to the Ref. [7], for $C \in (C_g, C_f)$ generalized synchronization takes place. The examples of phase portraits of the mapping (φ_n, ψ_n) for hyperchaotic and generally synchronous chaotic regimes are shown in Figs. 4b and 4c, respectively. In Fig. 4b one can observe the crowding of the phase trajectories in the regions aside from the diagonal, that is similarly to Fig. 2c for the system (2.1), (2.4). For the case of the generally synchronous regime, the phase portrait in Fig. 4c represents a diffuse strip parallel with the diagonal, that agrees well with the prediction of the discrete model. Note, that the diffusion occurs due to intrinsic nonlinearity of the basic subsystem (3.1). We would obtain a similar diagram for the system (2.1) by adding a nonlinear term into the Bernoulli map. It is also significant that the generally synchronous regime is bistable, i.e., starting integration of the system (3.2), (3.4) with another set of initial conditions, we can obtain the phase portrait analogous to the one presented in Fig. 4c, but reflex with respect to the diagonal. The last also agrees with the results for the model (2.1), (2.4). As the parameter C is further increased, the diffuse strips become sharpen and

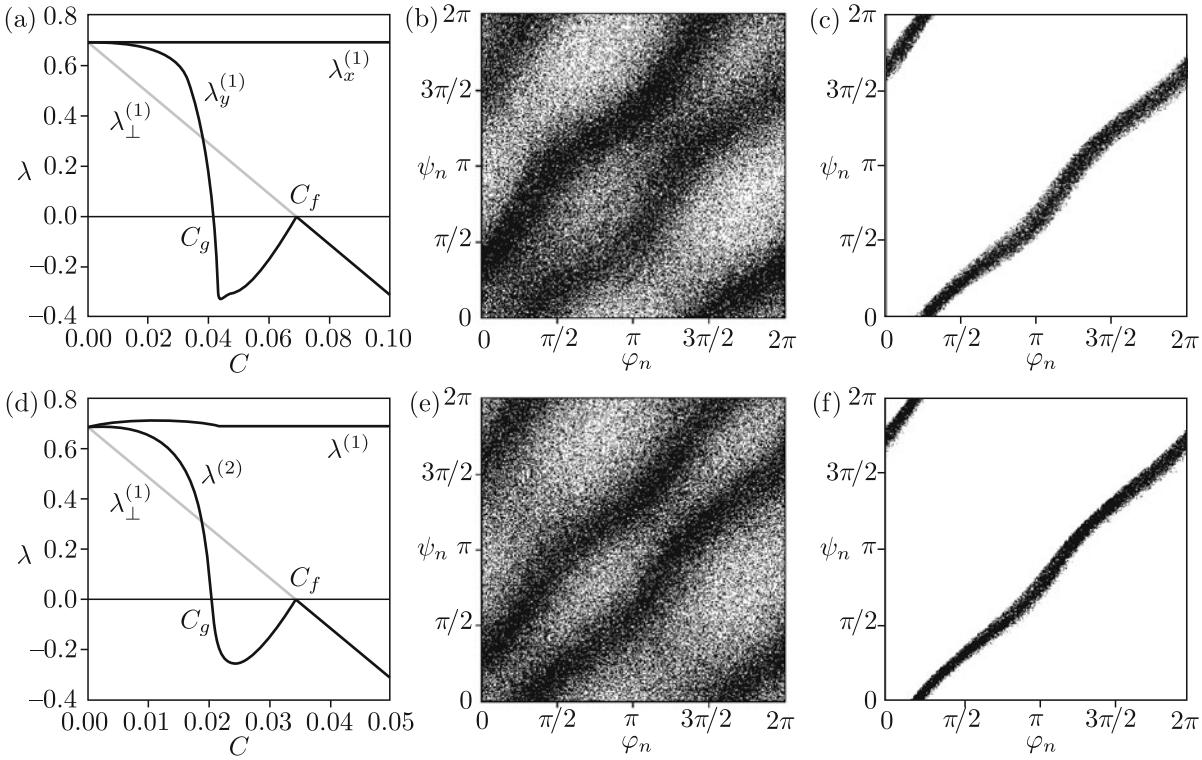

Fig. 4. (a) The dependences of Lyapunov exponents of the system (3.2),(3.4) with unidirectional nonlinear coupling ($\alpha = 1, B = 0.007$) vs. parameter C, and the phase portraits of the mapping (φ_n, ψ_n): (b) for hyperchaotic regime at $C = 0.035$, and (c) for generally synchronous chaotic regime at $C = 0.050$. (d) The dependences of Lyapunov exponents of the system (3.2), (3.4) with symmetric nonlinear coupling ($\alpha = 0, B = 0.015$) vs. parameter C, and the phase portraits of the mapping (φ_n, ψ_n): (e) for hyperchaotic regime at $C = 0.015$, and (f) for generally synchronous chaotic regime at $C = 0.022$.

finally merge with the diagonal at $C = C_f$, when the manifold M becomes transversally stable and the complete synchronization appears.

The entirely analogous picture of the transition takes place for symmetrically coupled systems. Unfortunately, it is impossible to establish the existence of the generalized synchronization strictly in this case, since there is no response system for mutual coupling, and we can not distinguish the largest Lyapunov exponent associated with this system. However, the transition of the second exponent $\lambda^{(2)}$ of the whole system (see Fig. 4d, $\lambda^{(2)}$ is shown in black) into the region of negative values at $C = C_g \approx 0.0205$ gives evidence on a qualitative change of the system's dynamics, namely, on the hyperchaos-to-chaos transition. The phase portrait in coordinates (φ_n, ψ_n) for hyperchaotic regime on the threshold of this transition (Fig. 4e) shows the crowding of phase trajectories in the regions aside from the diagonal. The portrait of generally synchronous regime has the form of the diffuse strip, which is parallel to the diagonal (Fig. 4f), as it was predicted by the discrete model. Note, that this regime is also bistable. Finally, as in the previous cases, the transition to the complete synchronization occurs in the moment when $\lambda_\perp^{(1)}$ passes the zero value and the manifold M becomes transversally stable.

4. CONCLUSION

In the present paper we have studied two general scenarios of the appearance of complete synchronization for coupled identical chaotic subsystems. In accordance with one of the, the generalized synchronization plays the role of the intermediate type of the dynamics on the route of the transition from asynchronous hyperchaotic behavior to the complete synchrony. According to the another scenario, the direct transition from asynchronous hyperchaos to complete synchrony takes place. It is shown, that the realization of one or another scenario is caused by the order

of appearance of transversal stability on the manifold of identically synchronous states and in the neighboring regions of the phase space under variation of the controlling parameter of the transition. In the case when the transversal stability appears first on the manifold of the identically synchronous states, and only then it extends upon the manifold's neighborhood, the direct transition from asynchronous hyperchaos to completely synchronous chaos is observed. On the other hand, if the local transversal stability of the trajectories appears first in the regions containing chaotic attractor and being distant from the manifold, and only then the manifold becomes transversally stable, the generalized synchronization arises. The mechanism of the birth of generally synchronous attractor is analogous to the saddle-node bifurcation. The obtained results are common for both unidirectionally and mutually coupled system, as shown for discrete modeling maps and feasible flow models of the oscillatory type.

In conclusion we would like to note, that coupled identical chaotic systems represent a convenient model for the investigation of the mechanisms not of the complete synchronization only, but also for the study of generalized, phase and, possibly, some other types of chaotic synchronization, and different transition between these types of dynamics.

ACKNOWLEDGMENTS

The author thanks Prof. A. Pikovsky and Prof. S. Kuznetsov for useful discussions. The work is supported by RFBR grant No. 12-02-00342.

REFERENCES

1. Fujisaka, H. and Yamada, T., Stability Theory of Synchronized Motion in Coupled-Oscillator Systems, *Progr. Theoret. Phys.,* 1983, vol. 69, no. 1, pp. 32–47.
2. Afraimovich, V. S., Verichev, N. N., and Rabinovich, M. I., Stochastic Synchronization of Oscillation in Dissipative Systems, *Izv. Vyssh. Uchebn. Zaved. Radiofiz.,* 1986, vol. 29, no. 9, pp. 1050–1060 [*Radiophys. Quantum Electron.,* 1986, vol. 29, pp. 795–802].
3. Pikovsky, A. S., On the Interaction of Strange Attractors, *Z. Phys. B,* 1984, vol. 55, no. 2, pp. 149–154.
4. Pecora, L. M. and Carroll, T. L., Synchronization in Chaotic Systems, *Phys. Rev. Lett.,* 1990, vol. 64, no. 8, pp. 821–824.
5. Pecora, L. M. and Carroll, T. L., Driving Systems with Chaotic Signals, *Phys. Rev. A,* 1991, vol. 44, no. 4, pp. 2374–2383.
6. Rulkov, N. F., Sushchik, M. M., Tsimring, L. S., and Abarbanel, H. D. I., Generalized Synchronization of Chaos in Directionally Coupled Chaotic Systems, *Phys. Rev. E,* 1955, vol. 51, no. 2, pp. 980–994.
7. Kocarev, L. and Parlitz, U., Generalized Synchronization, Predictability and Equivalence of Unidirectionally Coupled Systems, *Phys. Rev. Lett.,* 1996, vol. 76, no. 11, pp. 1816–1819.
8. Hunt, B. R., Ott, E., and Yorke, J. A., Differentiable Generalized Synchronization of Chaos, *Phys. Rev. E,* 1997, vol. 55, no. 4, pp. 4029–4034.
9. Boccaletti, S., Kurths, J., Osipov, G., Valladares, D. L., and Zhou, C. S., The Synchronization of Chaotic Systems, *Phys. Rep.,* 2002, vol. 366, nos. 1–2, pp. 1–101.
10. Brown, R. and Kocarev, L., A Unifying Definition of Synchronization for Dynamical Systems, *Chaos,* 2000, vol. 10, no. 2, pp. 344–349.
11. Abarbanel, H. D. I., Rulkov, N. F., and Sushchik, M. M., Generalized Synchronization of Chaos: The Auxiliary System Approach, *Phys. Rev. E,* 1996, vol. 53, no. 5, pp. 4528–4535.
12. Parlitz, U., Junge, L., and Kocarev, L., Nonidentical Synchronization of Identical Systems, *Internat. J. Bifur. Chaos Appl. Sci. Engrg.,* 1999, vol. 9, no. 12, pp. 2305–2309.
13. González-Miranda, J. M., Generalized Synchronization in Directionally Coupled Systems with Identical Individual Dynamics, *Phys. Rev. E,* 2002, vol. 65, no. 4, 047202, 4 pp.
14. Uchida, A., McAllister, R., Meucci, R., and Roy, R., Generalized Synchronization of Chaos in Identical Systems with Hidden Degrees of Freedom, *Phys. Rev. Lett.,* 2003, vol. 91, no. 17, 174101, 4 pp.
15. Pyragas, K., Weak and Strong Synchronization of Chaos, *Phys. Rev. E,* 1996, vol. 54, no. 5, R4508–R4511.
16. Shabunin, A., Astakhov, V., and Kurths, J., Quantitative Analysis of Chaotic Synchronization by Means of Coherence, *Phys. Rev. E,* 2005, vol. 72, no. 1, 016218, 11 pp.
17. Shabunin, A. V., Astakhov, V. V., Demidov, V. V., and Efimov, A. V., Multistability and Synchronization of Chaos in Maps with "Internal" Coupling, *Radiotekhnika i Elektronika,* 2008, vol. 53, no. 6, pp. 702–712 [*J. Commun. Technol. Electr.,* 2008, vol. 53, no. 6, pp. 666–675].
18. Yanchuk, S., Maistrenko, Yu., and Mosekilde, E., Synchronization of Time-Continuous Chaotic Oscillators, *Chaos,* 2003, vol. 13, no. 1, pp. 388–400.
19. Neumann, E., Sushko, I., Maistrenko, Yu., and Feudel, U., Synchronization and Desynchronization under the Influence of Quasiperiodic Forcing, *Phys. Rev. E,* 2003, vol. 67, no. 2, 026202, 15 pp.

20. de Sousa Vieira, M. and Lichtenberg, A. J., Nonuniversality of Weak Synchronization in Chaotic Systems, *Phys. Rev. E,* 1997, vol. 56, no. 4, R3741–R3744.
21. Tamasevicius, A. and Cenys, A., Synchronizing Hyperchaos with a Single Variable, *Phys. Rev. E,* 1997, vol. 55, no. 1, pp. 297–299.
22. Gauthier, D. J. and Bienfang, J. C., Intermittent Loss of Synchronization in Coupled Chaotic Oscillators: Toward a New Criterion for High-Quality Synchronization, *Phys. Rev. Lett.,* 1996, vol. 77, no. 9, pp. 1751–1754.
23. Junge, L. and Parlitz, U., Synchronization Using Dynamic Coupling, *Phys. Rev. E,* 2001, vol. 64, no. 5, 055204(R), 4 pp.
24. Pikovsky, A. S. and Grassberger, P., Symmetry Breaking Bifurcation for Coupled Chaotic Attractors, *J. Phys. A,* 1991, vol. 24, no. 19, pp. 4587–4597.
25. Ding, M. and Yang, W., Observation of Intermingled Basins in Coupled Oscillators Exhibiting Synchronized Chaos, *Phys. Rev. E,* 1996, vol. 54, no. 3, pp. 2489–2494.
26. Maistrenko, Yu. L., Maistrenko, V. L., Popovich, A., and Mosekilde, E., Transverse Instability and Riddled Basins in a System of Two Coupled Logistic Maps, *Phys. Rev. E,* 1998, vol. 57, no. 3, pp. 2713–2724.
27. Kuznetsov, S. P., Example of a Physical System with a Hyperbolic Attractor of the Smale–Williams Type, *Phys. Rev. Lett.,* 2005, vol. 95, 144101, 4 pp.
28. Kuznetsov, S. P. and Seleznev, E. P., A Strange Attractor of the Smale–Williams Type in the Chaotic Dynamics of a Physical System, *Zh. Eksper. Teoret. Fiz.,* 2006, vol. 129, no. 2, pp. 400–412 [*J. Exp. Theor. Phys.,* 2006, vol. 102, no. 2, pp. 355–364].